Title

Seismic-Induced Deformations of a Geosynthetic Reinforced Soil Bridge Abutment Subjected to Longitudinal Shaking

Authors

Rong, Wenyong
Zheng, Yewei
McCartney, John S
et al.

Publication Date

2018-06-06

DOI

10.1061/9780784481608.015

Peer reviewed

Seismic-induced Deformations of a Geosynthetic Reinforced Soil Bridge Abutment Subjected to Longitudinal Shaking

Wenyong Rong[1], M.S., S.M.ASCE, Yewei Zheng[2], Ph.D., A.M.ASCE
John S. McCartney[3], Ph.D., P.E., M.ASCE, Patrick J. Fox[4], Ph.D., P.E., F.ASCE

[1]Graduate Research Assistant, Department of Structural Engineering, University of California San Diego, La Jolla, CA 92093-0085; Email: w1rong@eng.ucsd.edu
[2]Postdoctoral Research Scholar, Department of Structural Engineering, University of California San Diego, La Jolla, CA 92093-0085; Email: y7zheng@ucsd.edu
[3]Associate Professor, Department of Structural Engineering, University of California San Diego, La Jolla, CA 92093-0085; Email: mccartney@ucsd.edu
[4]Shaw Professor and Head, Department of Civil and Environmental Engineering, Pennsylvania State University, University Park, PA 16802; Email: pjfox@engr.psu.edu

ABSTRACT

Although Geosynthetic-Reinforced Soil (GRS) bridge abutments have been used widely in highway infrastructure projects, understanding their response during earthquake loading is a remaining issue that is affecting their implementation throughout the United States. In particular, the 3-dimensional (3D) seismic response of GRS bridge abutments is critical to consider as the direction of shaking in the field may be uncertain and because experimental work has shown that it is possible to have horizontal deformations in directions other than the primary direction of shaking. Further, any horizontal deformations of the GRS bridge abutment may be linked with settlements of the bridge seat, so 3D deformations are important to understand. This study involves 3D numerical simulations of the seismic response of a hypothetical GRS bridge abutment experiencing 1-dimensional horizontal shaking in the longitudinal direction of the bridge beam, focusing on the lateral deformations of the GRS bridge abutment in the longitudinal and the transverse directions. Time histories of the horizontal deformations in both directions are presented and synthesized with settlements of the bridge seat to evaluate the applicability of using the Federal Highway Administration (FHWA) design method linking vertical and lateral static deformations by assuming zero-volume change in the GRS mass to seismic loading.

INTRODUCTION

Geosynthetic-reinforced soil (GRS) bridge abutments are widely used as alternatives to conventional pile-supported bridge abutments for they offer a competitive solution in terms of cost effectiveness, faster construction, as well as good performance under static and seismic conditions (Helwany et al. 2003). GRS bridge abutments generally include a lower GRS supporting a bridge seat (i.e., a shallow footing) upon which the bridge beam rests and an upper GRS wall supporting the approach slab for the roadway connection. The Federal Highway Administration (FHWA) developed design guidelines for GRS bridge abutments, and presented a method to estimate the lateral deformations of the GRS bridge abutment from the vertical settlement during static loading (Adams et al. 2011). Specifically, the lateral facing displacement

is estimated from the vertical settlement by assuming a zero-volume change in the GRS mass and the expected shape of the lateral deformation profile. This approach is expected to lead to a conservative estimate of the lateral facing displacement for static loading, but it has not been fully confirmed. Plane strain stress state was used as the basis for this assumption, which may not be the case when considering the lateral facing displacements of GRS bridge abutments in the transverse and longitudinal directions, and, it is not clear if this assumption will be applicable to seismic conditions.

The static deformation behavior of GRS bridge abutments has been studied extensively using numerical simulations (Helwany et al. 2007; Wu et al. 2006; Zheng and Fox 2016; Rong et al. 2017), which all indicated satisfactory performance under service loads. Results from these studies indicate that a 3D deformation response is expected during static loading due to the boundary constraints of the GRS bridge abutment. Rong et al. (2017) investigated three cases of GRS bridge abutments with different reinforcement lengths and vertical spacing, and the relationship between the volume decrease of the reinforced soil element beneath the bridge beam due to bridge seat settlement and the volume increase of the element due to lateral facing displacements is shown in Figure 1. The volume increase values for the three cases were lower than those predicted from the bridge seat settlement using the FHWA assumption of zero-volume change. This is consistent with the expectation of Adams et al. (2011) that the FHWA method would yield a conservative estimate for static loading.

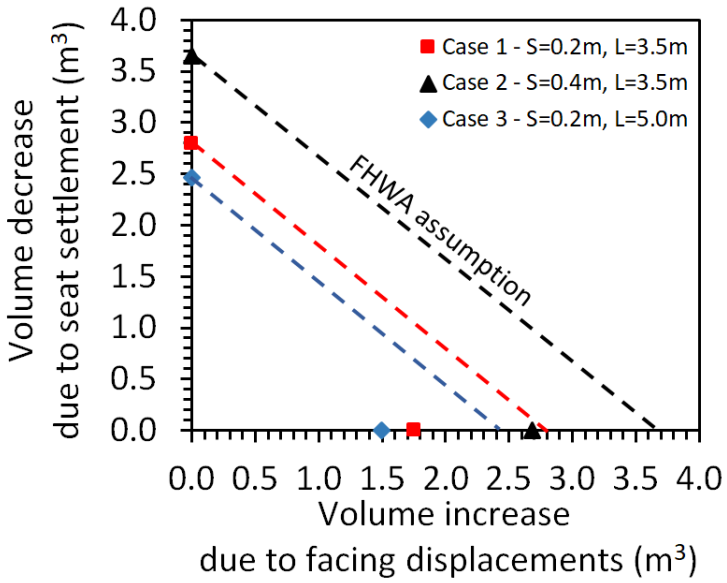

Figure 1. Evaluation of the FHWA zero-volume change assumption for static loading of a 3D bridge abutment (data from Rong et al. 2017)

A limited set of field data on GRS bridge abutments also indicate satisfactory performance in static conditions. For example, the extensively instrumented Founders/Meadows Bridge in Castle Rock, CO (Abu-Hejleh et al. 2002) experienced a maximum facing displacement of 10 mm for the front wall (in the longitudinal direction) and a maximum settlement of 13 mm for the bridge seat during construction. Helwany et al. (2012) performed full-scale shaking table tests on a 3.6

m-high GRS bridge abutment subjected to a series of sinusoidal motions with increasing amplitudes up to 1 g and found little damage to the abutments until horizontal acceleration reached 0.67 g. However, they did not report the deformations of the side walls in the transverse direction. Experimental work has shown that it is possible to have horizontal deformations in directions other than the primary direction of shaking. For example, Zheng et al. (2017) conducted half-scale shaking table tests on a 2.7 m-high GRS bridge abutment subjected to two earthquake motions and found the model system performed well, with a maximum residual facing displacement of -1.0 mm (with a negative sign denoting outward displacement) and an average bridge seat settlement of 1.4 mm (with a positive sign denoting downward movement), respectively, as shown in Figure 2. Although earthquake motion was applied in the longitudinal direction, the results in Figure 2 indicate facing displacements were observed in both the longitudinal and transverse directions. The peak and residual displacements are similar in magnitude in the longitudinal and transverse directions.

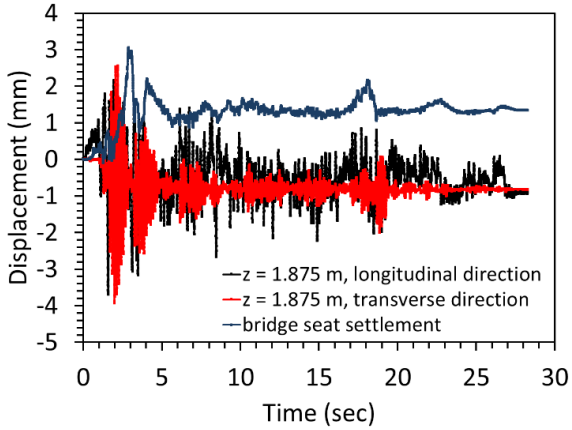

Figure 2. Time histories of facing displacements and bridge seat settlement due to scaled 1940 Imperial Valley earthquake motion (results in model-scale)

NUMERICAL MODEL

In this study, a 3D model of a hypothetical GRS bridge abutment previously studied by Rong et al. (2017) for static loading conditions was simulated to study 3D dynamic deformations of the abutment subjected to an earthquake motion in the longitudinal direction. This analysis evaluates the applicability of zero-volume change assumption of soil mass in GRS bridge abutment proposed by FHWA for static conditions to seismic conditions. The finite difference computer program FLAC 3D version 5.0 (Itasca 2012) was used to simulate the dynamic response of GRS bridge abutments. Geogrid structural elements were used to model reinforcements and interface elements were used to model interactions between different components, including soil-concrete interface and concrete-concrete interface. Interface elements were characterized using the Coulomb sliding block model. The GRS bridge abutment involved simulation of staged construction to develop the initial stress states, after which dynamic analysis was performed with the 1940 Imperial Valley ground motion (recorded at the El Centro station) applied at the GRS bridge abutment foundation in the longitudinal direction.

Model Configuration

The configuration for the GRS bridge abutment model with marked components and the finite difference mesh is shown in Figure 3. The bridge has a span of 16 m, width of 8 m, bridge beam thickness of 0.85 m, bridge seat thickness of 0.4 m, bridge contact length of 0.85 m, lower GRS wall height of 3 m (H), upper GRS wall height of 1.25 m, total abutment height of 4.25 m, foundation soil depth of 6 m ($2H$), distance of lower wall facing to lateral boundaries of 9 m ($3H$), and 100 mm wide expansion joint between the bridge beam and bridge seat on each side. The GRS wall facing consists of modular block concrete elements that measure 0.5 m (length) × 0.25 m (width) × 0.2 m (height). The bridge abutment consists of a bridge seat that measures 9 m (width) × 1.35 m (length) × 1.25 m (height), and sits on top of a soil mass measuring 8.75 m and 10.5 m in the longitudinal and transverse directions respectively, and offset 0.2 m from the back of the lower front wall facing in the longitudinal direction and 0.75 m from the back of the lower side wall facing in the transverse direction.

Each reinforcement layer includes one geogrid placed longitudinally and two geogrids placed transversely. Geogrid reinforcements for the lower and upper wall having the same length 2.1 m ($0.7H$) and the same vertical spacing 0.2 m are rigidly connected to the facing blocks with the upper reinforcements rigidly connected to the back of the bridge seat in the longitudinal direction. With an equivalent unit weight of 23.52 kN/m^3 for the bridge structure, the corresponding average applied vertical stress on the bridge seat is 188 kPa. Since the bottom surface area of the bridge seat (1.35 m × 9 m) is greater than the bridge contact area (0.85 m × 8 m), the average vertical stress on the backfill soil is 105 kPa [(160 kN/m × 8 m) / (1.35 m × 9 m)]. The lateral boundaries for the model in the x and y directions were located at distances of 9 m and 5 m away from the lower wall facing blocks to minimize any boundary effects during staged construction and the subsequent earthquake shaking.

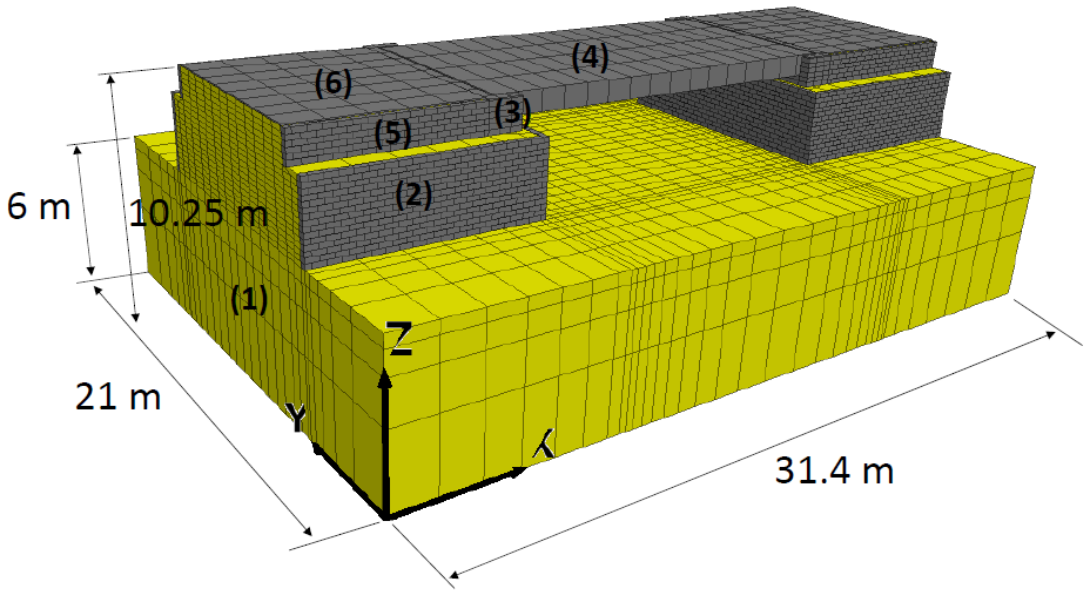

Figure 3. Finite difference model configuration for the GRS bridge abutment (1: foundation soil, 2: lower GRS wall, 3: bridge seat, 4: bridge beam, 5: upper GRS wall, 6: pavement).

Material Models and Properties

The concrete facing blocks, bridge seat, bridge beam and approach slabs were modeled as linearly elastic materials having Young's modulus E = 20 GPa and Poisson's ratio v = 0.2. The foundation and the reinforced soil mass were modeled as linearly-elastic perfectly-plastic dilatant material with a Mohr-Coulomb failure criterion and non-associated flow rule with a Young's modulus E = 50 MPa, a Poisson's ratio v = 0.3. The total density of the soil was assumed to be 2000 kg/m^3. Interfaces were modeled using coulomb sliding model with proper normal and shear stiffness values within FLAC 3D preventing penetration of the model grids but allowing sliding or separation between them during earthquake shaking. Typical values were selected for these constitutive model parameters and the details can be found in Rong et al. (2017).

Mechanical damping is an important consideration in dynamic analysis. For earth materials, damping commonly falls in the range of 2% to 5% of critical (Biggs 1964). A considerable amount of energy dissipation can occur during plastic flow for the foundation soils and the backfills assigned with a plasticity Mohr-Coulomb constitutive model in this study. Thus, for dynamic analysis involving large-strain, only a minimal percentage of damping may be required. Local damping was originally designed as an approach to equilibrate static simulation in FLAC 3D. However, it has some characteristics that make it attractive for dynamic simulations if the frequency content of the applied earthquake motion falls in a narrow range. It operates by adding or subtracting mass from a gridpoint or structural node at certain times during a cycle of oscillation and reduces the computation effort remarkably. Therefore, in this study, local damping was used as an approximate way to consider the energy loss in the model. The amount of energy removed ΔW is proportional to the maximum strain energy W and the ratio $\Delta W/W$ is independent of rate and frequency. Since $\Delta W/W$ may be related to fraction of critical damping D (Kolsky 1963), the following expression is used to obtain the local damping coefficient α_L,

$$\alpha_L = \pi D \tag{1}$$

Thus, implementation of local damping is much simpler than Rayleigh damping for there is no need to specify the natural frequency of the system and it reduces the computation effort remarkably. A typical damping ratio value of 5% was selected in the following dynamic analysis, which lead to the local damping coefficient of 0.1571.

Dynamic Loading and Boundary Conditions

Numerical analysis of the dynamic response of geotechnical structures such as earth dams and bridge abutments require the discretization of a region of the materials adjacent to the foundation. The seismic input motion is normally represented by plane waves propagating upward through the underlying foundation. The boundary conditions at the sides of the model must account for the free-field motion that would exist in the absence of the earth structures. These boundaries should be placed at distances sufficient to minimize wave reflection and

achieve free-field conditions. For soils with high material damping, this condition can be obtained with a relatively small distance (Seed et al. 1975). However, when the material damping is low, the required distance may lead to an impractical numerical model. An alternative procedure involving the execution of free-field calculations in parallel with the main grids analysis was developed in FLAC 3D to enforce the free-field motion in such a way that boundaries retain their nonreflecting properties.

The input motion was applied at the base of the model in the longitudinal direction with zero accelerations in other directions. The 1940 Imperial Valley earthquake ground motion recorded at the El Centro station was selected to apply at the base of the model in the longitudinal direction, which is shown in Figure 4(a). The duration of this ground motion history was around 40 s, and the Peak Ground Acceleration (PGA) was 0.31 g (at 2.2 s). Numerical distortion of the propagation wave can occur in a dynamic analysis as a function of the modeling function. Kuhlemeyer and Lysmer (1973) showed that, for accurate wave transmission through a model, the spatial element size ΔL must be smaller than approximately one-tenth to one-eighth of the wave length associated with the highest frequency component of the input motion, as follows:

$$\Delta L \leq \frac{\lambda}{10} \tag{2}$$

where λ is the wavelength associated with the highest frequency component that contains appreciable energy. Therefore, the frequency content of the input motion was analyzed first to determine the proper size of the mesh grid for accurate wave propagation. To evaluate the frequency content, the input motion was evaluated in the form of velocity time history for the induced stress in the model is directly proportional to velocity. After Fast Fourier Transform (FFT) of the integration of the input acceleration time history, the frequency content of the input velocity is shown in Figure 4(b).

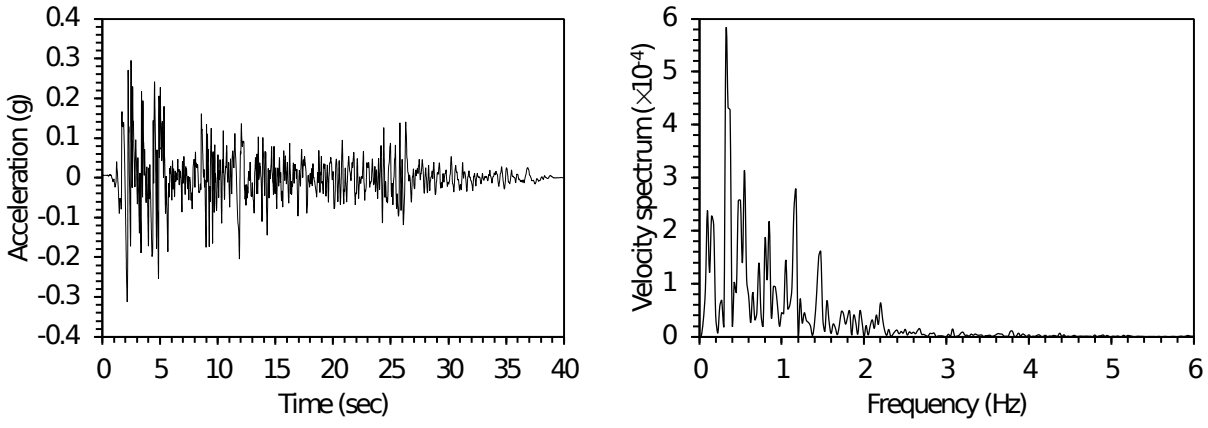

(a) (b)

Figure 4. Applied input earthquake ground motion (1940 Imperial Valley earthquake): (a) Acceleration time history; (b) Frequency content of the velocity time history.

Most of the power for the input motion is contained in the lower frequency component (≤ 2.4

Hz). For the backfill soil properties, the average shear wave velocity within the GRS wall is:

$$V_s = \sqrt{\frac{G}{\rho}} = 98\, m/s \tag{3}$$

which can be used to calculate the wavelength λ associated with the highest frequency component, as follows:

$$\lambda = \frac{V_s}{f} = 40.8\, m \tag{4}$$

Therefore, the spatial grid size in the 3D model must be smaller than 4.08 m to ensure accurate wave propagation.

Modeling Procedures

Staged construction of the GRS bridge abutment was simulated to reach equilibrium state first under self-weight so that initial stress state of the model can be developed prior to seismic excitation. The construction sequence of the GRS bridge abutment was performed by first placing the foundation soil. Large-strain mode was then turned on during the next staged construction to ensure sufficient accuracy for possible large deformations. The lower GRS wall, including 25 soil lifts, reinforcements, and concrete facing blocks was placed layer by layer and simulated to equilibrium state with added interfaces between the facing blocks and between the facing block and backfill soil. Then the bridge seat was placed on the reinforced soil masses on either side of the bridge beam and the bridge beam was placed on the seat. Finally, the upper 13 lifts of backfill in the upper GRS wall were placed, followed by the 50 mm-thick approach roadways, following the same approach used for the lower GRS wall. With the developed initial stress state and free-field boundary conditions, the 1940 Imperial Valley earthquake motion shown in Figure 3(a) was applied at the base of the model in the longitudinal direction (x) with zero accelerations in the other two directions (y and z). Large strains were permitted to consider any physical interface sliding and failure modes.

SIMULATION RESULTS

Simulation results of the 3D model described above under the 1940 Imperial Valley earthquake motion are presented in this section. Only the left GRS bridge abutment is discussed. Incremental horizontal dynamic displacements of facing blocks at different elevations (z = 0.2 m, 0.6 m, 1.0 m, 1.4 m, 1.8 m, 2.2 m, 2.6 m) of the longitudinal centerline section and the transverse section under the bridge seat were recorded, along with the average bridge seat settlement. Facing displacements at several representative elevations in the longitudinal and transverse directions are shown in Figures 5(a) and 5(b), respectively. The average bridge seat settlement is shown in Figure 5(c). In the current model, facing blocks in both directions were pushed outward at the start of intense shaking at a time of around t = 2 s with the bridge seat responded simultaneously to some extent.

Maximum and residual facing displacements at different elevations are shown in Figure 6. The residual displacements of the recorded blocks were very close to their maximum responses. Further, the residual displacements of the facing blocks in the longitudinal direction increased gradually with height, and the maximum facing displacement was 68 mm at z = 2.6 m.

Pronounced displacements of the transverse section happened, although the earthquake motion was applied longitudinally. Maximum displacement of the transverse section happened near the top, and it was 16 mm at z = 1.8 m while the average residual displacement of this transverse section was around 12 mm.

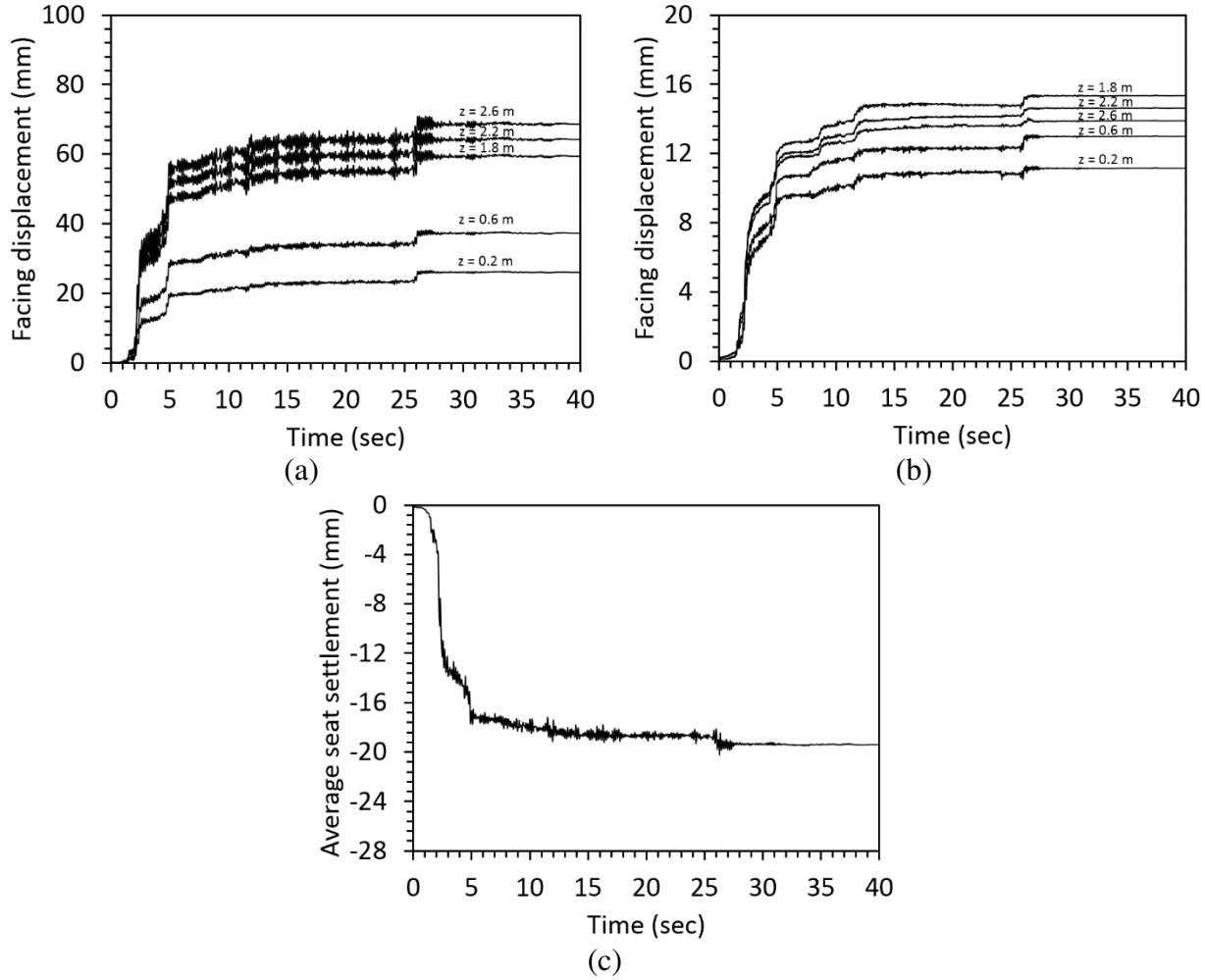

Figure 5. Time series of recorded horizontal displacements and bridge seat settlement: (a) Longitudinal centerline section; (b) Transverse section under the bridge seat; (c) Average bridge seat settlement.

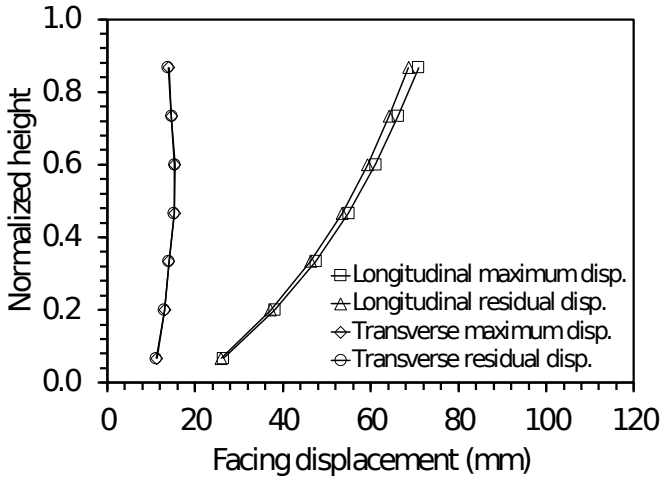

Figure 6. Simulated profiles of the maximum and residual horizontal facing displacements

Evaluation of the time histories in Figure 5 indicates there might be a linkage between the settlement of the bridge seat and the outward displacements of the abutment walls. When the abutment walls were pushed out in the longitudinal and transverse directions intensively, a settlement of the bridge seat was observed simultaneously. Volume changes of the reinforced soil mass directly under the bridge seat due to the outward facing displacements and downward bridge seat settlement were shown and compared with the prediction of the lateral facing displacement from the FHWA assumption in Figure 7. The displacement profiles in Figure 6 were used to calculate the volume increases due to the outward facing displacements of the longitudinal and the transverse sections. Since the earthquake motion was applied in the longitudinal direction, displacement profiles of the side walls in the transverse direction were assumed to be symmetric. The volume decrease due to seat settlement was 0.4 m^3, while the volume increase due to outward facing displacements in the longitudinal and transverse directions was about 1.0 m^3. Results in this study indicate that zero-volume change assumption for static loading conditions may not be applicable to seismic loadings. The lateral facing displacements estimated from the bridge seat settlement will be smaller than those observed in the 3D simulations, which is unconservative. This indicates that the zero-volume change assumption in the FHWA method may not be applicable to seismic conditions, although the reasons for this discrepancy need a deeper analysis.

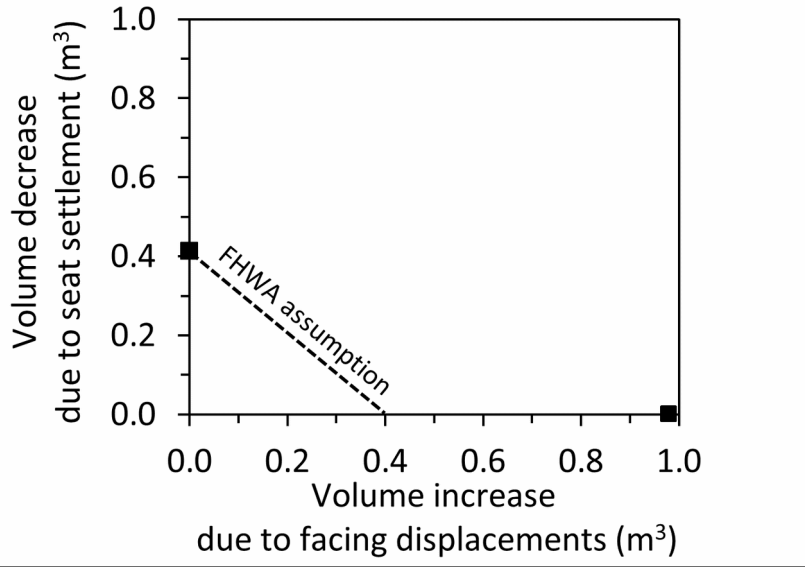

Figure 7. Volume changes of the GRS mass beneath the bridge seat, with predicted trends based on the FHWA assumption of zero volume change.

CONCLUSIONS

The seismic response of a hypothetical GRS bridge abutment under the 1940 Imperial Valley earthquake motion was simulated using finite difference program FLAC 3D. Although the earthquake motion was applied in the longitudinal direction, lateral deformations of the lower GRS bridge abutment in both the longitudinal and transverse directions are appreciable and cannot be ignored. The bridge seat settlement and outward facing displacements of the abutment wall may be related, but the estimate following the zero-volume change of the soil mass may not be conservative for seismic conditions as it is for static conditions. Further research involving simulation with calibrated soil model should be conducted and validated against case histories.

ACKNOWLEDGEMENTS

Financial support was provided by the California Department of Transportation (Caltrans) and is gratefully acknowledged. We also thank Dr. Charles S. Sikorsky of the Caltrans Office of Earthquake Engineering for his support and assistance with the project.

REFERENCES

Abu-Hejleh, N., Zornberg, J.G., Wang, T., and Watcharamonthein, J. (2002). "Monitored displacements of unique geosynthetic-reinforced soil bridge abutments." Geosynthetics International, 9(1), 71-95.

Adams, M., Nicks, J., Stabile, T., Wu, J., Schlatter, W., and Hartmann, J. (2011). Geosynthetic Reinforced Soil Integrated Bridge System. Synthesis Report No. FHWA-HRT-11-027.

Biggs, J.M. (1964). "Introduction to Structural Dynamics." New York: McGraw-Hill.

Helwany, S.M., Wu, J.T., and Froessl, B. (2003). "GRS bridge abutments-an effective means to alleviate bridge approach settlement." Geotextiles and Geomembranes, 21(3), 177-196.

Helwany, S.M., Wu, J.T., and Kitsabunnarat, A. (2007). “Simulating the behavior of GRS bridge abutments.” Journal of Geotechnical and Geoenvironmental Engineering, 133(10), 1229-1240.

Helwany, S.M.B., Wu, J.T.H., and Meinholz, P. (2012). “Seismic design of geosynthetic reinforced soil bridge abutments with modular block facing.” NCHRP Web-Only Document 187, Transportation Research Board, Washington, D.C., USA.

Iai, S. (1989) “Similitude for shaking table tests on soil-structure-fluid models in 1 g gravitational fields,” Soils and Foundations, 29(1), 105-118.

Itasca Consulting Group, Inc. (2012). Fast Lagrangian Analysis of Continua in 3 Dimensions - 3D Version 5.0. Itasca Consulting Group, Inc., Minneapolis.

Kolsky, H. (1963). “Stress Waves in Solids.” New York: Dover Publications.

Kuhlemeyer, R.L., and Lysmer, J. (1973). “Finite element method accuracy for wave propagation problems.” Journal of Soil Mechanics and Foundations, Div, 99(SM5), 421-427.

Rong, W., Zheng, Y., McCartney, J.S., and Fox, P.J. (2017). “3D deformation behavior of a geosynthetic reinforced soil bridge abutment.” Geotechnical Frontiers 2017. Orlando, FL. ASCE. 44-55.

Seed, H.B., Martin, P.P., and Lysmer, J. (1975). “The generation and dissipation of pore water pressures during soil liquefaction.” College of Engineering, University of California.

Wu, J.T., Lee, K.Z., and Pham, T. (2006). “Allowable bearing pressures of bridge sills on GRS abutments with flexible facing.” Journal of Geotechnical and Geoenvironmental Engineering, 132(7), 830-841.

Zheng, Y., and Fox, P.J. (2016). “Numerical investigation of geosynthetic-reinforced soil bridge abutments under static loading.” Journal of Geotechnical and Geoenvironmental Engineering 142(5), 04016004.

Zheng, Y., Sander, A., Rong, W., McCartney, J.S., Fox, P.J., and Shing, P.B. (2017a). “Experimental design and setup for half-scale shake table test of a geosynthetic-reinforced soil bridge abutment.” Geotechnical Frontiers 2017. Orlando, FL. ASCE. 54-63.

Zheng, Y., Sander, A., Rong, W., Fox, P.J., Shing, P.B., and McCartney, J.S. (2017b). “Shaking table test of a half-scale geosynthetic-reinforced soil bridge abutment.” ASTM Geotechnical Testing Journal. https://doi.org/10.1520/GTJ20160268.